

Chapter 5

Tunneling Spectra of Electron-Doped $\text{Sr}_{1-x}\text{La}_x\text{CuO}_2$ ¹

5.1 Introduction

In the previous chapter, we have addressed the doping-dependent pairing symmetry, pairing potential and the spectral response to non-magnetic impurities in hole-doped (p-type) YBCO. Both the low-energy spectral characteristics of pure YBCO and the resonant impurity scattering spectra of the (Zn,Mg)-YBCO suggest that the superconducting order parameter is predominantly d -wave, with gapless nodal quasiparticles as the low-energy excitations. Furthermore, the significant increase of s -wave component in the overdoped Ca-YBCO and the pronounced high-energy satellite features in underdoped and optimally doped YBCO are indicative of their proximity to a quantum phase transition from the overdoped superconducting phase to the underdoped coexisting phase of superconductivity and a competing order. The satellite features that we interpret as a manifestation of the competing order evolve into the pseudogap above T_c in underdoped p-type cuprates. The commonly observed incommensurate spin-density-wave is one of the possible candidates for the competing order of the underdoped and optimally doped p-type cuprates.

The predominantly $d_{x^2-y^2}$ pairing symmetry [7, 6], the pseudogap phenomena [224, 9], and the existence of incommensurate spin fluctuations in the CuO_2 planes [224, 169] in the underdoped and optimally p-type cuprates have been widely conceived as essential to high-temperature supercon-

¹The main contents of this chapter are published as C.-T. Chen, *et al. Phys. Rev. Lett.* **88**, 227002 (2002).

ductivity. However, the pairing symmetry of the one-layer electron-doped (n-type) cuprates, such as $\text{Nd}_{1.85}\text{Ce}_{0.15}\text{CuO}_{4-\delta}$ (NCCO) and $\text{Pr}_{1.85}\text{Ce}_{0.15}\text{CuO}_{4-\delta}$ (PCCO), remains controversial [§1.2.1]. While the tunneling spectra of bicrystal grain-boundary junctions [40, 225] and point-contact tunneling spectroscopy [41] on nominally optimally doped NCCO report the absence of the zero-bias conductance peak along the $\{110\}$ direction and a momentum-independent pairing potential, tricrystal scanning SQUID magnetometry [43] on nominally optimally doped NCCO and PCCO and grain-boundary Josephson junction spectroscopy on nearly optimally doped $\text{La}_{2-x}\text{Ce}_x\text{CuO}_{4-y}$ ($x = 0.105$) (LCCO) [226] support the d -wave pairing symmetry. Results from the bulk penetration measurements have also been contradictory. Some experiments exhibit s -wave pairing in underdoped and nearly optimally doped PCCO [227, 228] while others reveal d -wave pairing [229, 230]. Furthermore, doping-dependent pairing symmetry is observed by point-contact spectroscopy [47] and penetration depth measurements [48], where the change from d -wave pairing in the underdoped to s -wave or $d + is(id')$ -pairing in optimally doped and overdoped one-layer PCCO has been suggested.

Concerning the pseudogap phenomena in the electron-doped cuprates, contrary to the normal-state low-energy spectral gap commonly observed in the hole-doped cuprates, no discernible loss of low-energy spectral weight above T_c has been demonstrated in quasiparticle tunneling spectroscopy of PCCO and NCCO [16, 17, 18]. On the other hand, magnetic-field-induced pseudogap-like features have been reported by tunneling spectroscopy on PCCO and LCCO in the normal state [17, 18], and these phenomena all occur below T_c in contrast to the findings in underdoped p-type cuprates. Moreover, no Nernst effect above $H_{c2}(T)$ or T_c has been found in any n-type cuprates, which is consistent with the absence of pseudogap phenomena. The behavior of the spin excitations in one-layer electron-doped cuprates is also distinctly different. While hole-doped cuprates display incommensurate low-energy spin fluctuations and an inward dispersion toward a magnetic resonance with increasing energy [231, 232], electron-doped NCCO [89] and $\text{Pr}_{0.88}\text{LaCe}_{0.12}\text{CuO}_{4-\delta}$ (PLCCO) [85, 92] display commensurate spin fluctuations with possible coexistence of a residual three-dimensional anti-ferromagnetic order [89, 233, 234].

A possible explanation for conflicting experimental observations of the pairing symmetry in n-

type cuprate superconductors is associated with difficulties in producing consistent material properties. Specifically, we note that in the growth of NCCO, PLCCO, and PCCO, it is necessary to subject the samples to a post-annealing oxygen reduction process in order to turn the non-superconducting as-grown crystals into superconductors. The uncertainty in the oxygen reduction renders a precise determination of the doping level difficult, and controversies arise over the nature of the charge carriers introduced to the CuO_2 planes because of possible self-doping of holes from the in-plane oxygen vacancies created by the oxygen reduction [235]. Besides, the formation of magnetic impurity phases during the reduction procedure casts doubts on some neutron scattering results [236]. The existence of magnetic ions, Nd^{3+} and Pr^{3+} , further complicates the interpretation of conflicting experimental observations of the one-layer electron-doped cuprates.

In comparison, the electron-doped infinite-layer cuprate $\text{Sr}_{0.9}\text{La}_{0.1}\text{CuO}_2$ (SLCO) is superior in that it contains only one metallic monolayer of Sr or La with no excess charge reservoir block between CuO_2 planes [Fig. 5.1]. The as-grown samples are free of magnetic ions and are superconducting without the need for oxygen reduction. Thus, scanning tunneling spectroscopy of SLCO should provide valuable information on the investigation of the asymmetry between n-type and p-type cuprates and on the universality of the pairing symmetry and pseudogap phenomena.

In this chapter, we report quasiparticle tunneling spectra of the n-type infinite-layer pure and impurity-doped SLCO that reveal characteristics which counter a number of common phenomena in the hole-doped cuprates. The nearly optimally doped SLCO with $T_c = 43$ K exhibits a momentum-independent superconducting gap $\Delta = 13.0 \pm 2.0$ meV that substantially exceeds the BCS value, and the spectral characteristics indicate the complete absence of satellite features above the spectral gap in the superconducting state and the absence of pseudogap in the normal state. The spectral response to quantum impurities at the Cu sites also differs fundamentally from that of the p-type cuprates with $d_{x^2-y^2}$ -wave pairing symmetry.

5.2 Crystalline structure and sample preparation

Despite significant progress in the studies of cuprate superconductivity, the research on the simplest form of cuprates, the infinite-layer system $\text{Sr}_{1-x}\text{Ln}_x\text{CuO}_2$ ($\text{Ln} = \text{La}, \text{Gd}, \text{Sm}$), has been limited [237, 238, 239] due to the difficulties in making single-phase bulk samples with complete superconducting volume. Recently, a breakthrough in high-pressure (4 GPa), high-temperature (950 C°) synthesis technique [240] has yielded single-phase polycrystalline samples of $\text{Sr}_{0.9}\text{La}_{0.1}\text{CuO}_2$ with nearly 100% superconducting volume and a sharp superconducting transition temperature at $T_c = 43$ K, thus enabling reliable spectroscopic studies of the pairing symmetry and the effects of quantum impurities.

These single-phased infinite-layer cuprates are n-type with P4/mmm symmetry, which differ significantly from other cuprates in that no excess charge reservoir block exists between consecutive CuO_2 planes except for a single layer of Sr (La) ions, as illustrated in Fig. 5.1. Contrary to the one-layer n-type cuprates, the oxygen distribution in the infinite-layer polycrystalline SLCO is perfectly stoichiometric, without oxygen vacancies in the CuO_2 planes and excess interstitial oxygen in the Sr (La) layer [237]. Furthermore, the c -axis superconducting coherence length ($\xi_c = 0.53$ nm) is found to be longer than the c -axis lattice constant ($c_0 = 0.347$ nm) [241], in stark contrast to other cuprate superconductors with $\xi_c \ll c_0$. Hence, the superconducting properties of the infinite-layer system are expected to be more three-dimensional, as opposed to the quasi-two-dimensional nature of all other cuprates.

The samples studied in this work included high-density granular samples of $\text{Sr}_{0.9}\text{La}_{0.1}\text{CuO}_2$ (SLCO), $\text{Sr}_{0.9}\text{La}_{0.1}(\text{Cu}_{0.99}\text{Zn}_{0.01})\text{O}_2$ (1% Zn-SLCO), and $\text{Sr}_{0.9}\text{La}_{0.1}(\text{Cu}_{0.99}\text{Ni}_{0.01})\text{O}_2$ (1% Ni-SLCO). X-ray diffraction (XRD) measurements confirm the single-phase nature of all samples, and both XRD and scanning electron microscopy (SEM) [240, 242] reveal random grain orientation and a typical grain size of a few micrometers in diameter. Magnetization studies reveal nearly 100% superconducting volume for all samples, with $T_c = 43$ K and $\Delta T_c \leq 1.0$ K for SLCO and 1% Zn-SLCO, and $T_c = 32$ K, $\Delta T_c \sim 1.0$ K for 1% Ni-SLCO. Structurally, the infinite-layer system is stoichiometrically homogeneous with up to < 3% Zn or Ni substitution [243].

The sample surface is prepared by non-aqueous chemical etching with 0.5% bromine in absolute

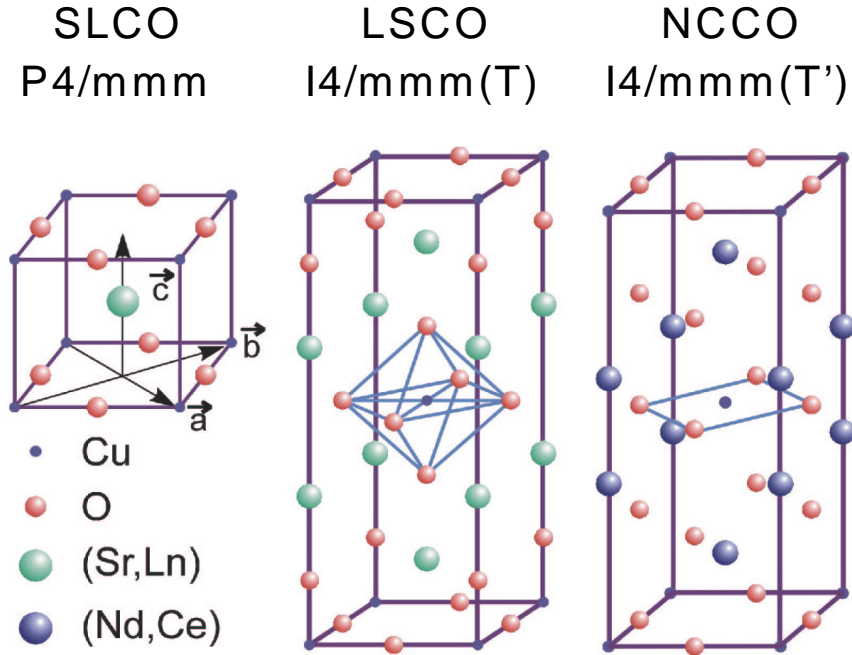


Figure 5.1: Comparison of the structure of the infinite-layer system $\text{Sr}_{1-x}\text{Ln}_x\text{CuO}_2$, ($\text{Ln} = \text{La}, \text{Gd}, \text{Sm}$), with those of the one-layer p-type (T-phase) and one-layer n-type (T'-phase) cuprates.

ethanol for less than 30 seconds [242], rinsed in pure ethanol, blown dry with high-purity helium or nitrogen, and transferred to the STM probe in a glove box with dry N_2 at ambient pressure. Nearly stoichiometric surface is confirmed with X-ray photoemission spectroscopy (XPS) [242]. We note that because of the polycrystalline nature of the sample, a shorter etching time is required in order to avoid damaging the grain boundaries and yielding disconnected crystallites on the surface.

5.3 Results of scanning tunneling spectroscopy

Quasiparticle tunneling spectra presented in this chapter are acquired with two low-temperature scanning tunneling microscopes, one of which is a solenoid-driven gas-cooled STM operating at 4.2 K, and the other is the variable-temperature shear-piezo-driven STM as described in Chapter 3. Tunneling spectra are taken on hundreds of randomly oriented grains for the three different infinite-layer compounds so as to sample a range of quasiparticle momenta relative to the crystalline axes of the local grains. A typical surface topography of the pure SLCO sample for our spectroscopic studies with sub-nanometer flatness is exemplified in the left panel of Fig. 5.2(a), and a zoom-out

view of this area is illustrated in Fig. 5.2(b). Confirming the local flatness for the tunneling spectra ensures that the average momentum of the incident quasiparticles relative to the crystalline axes of a grain is well-defined.

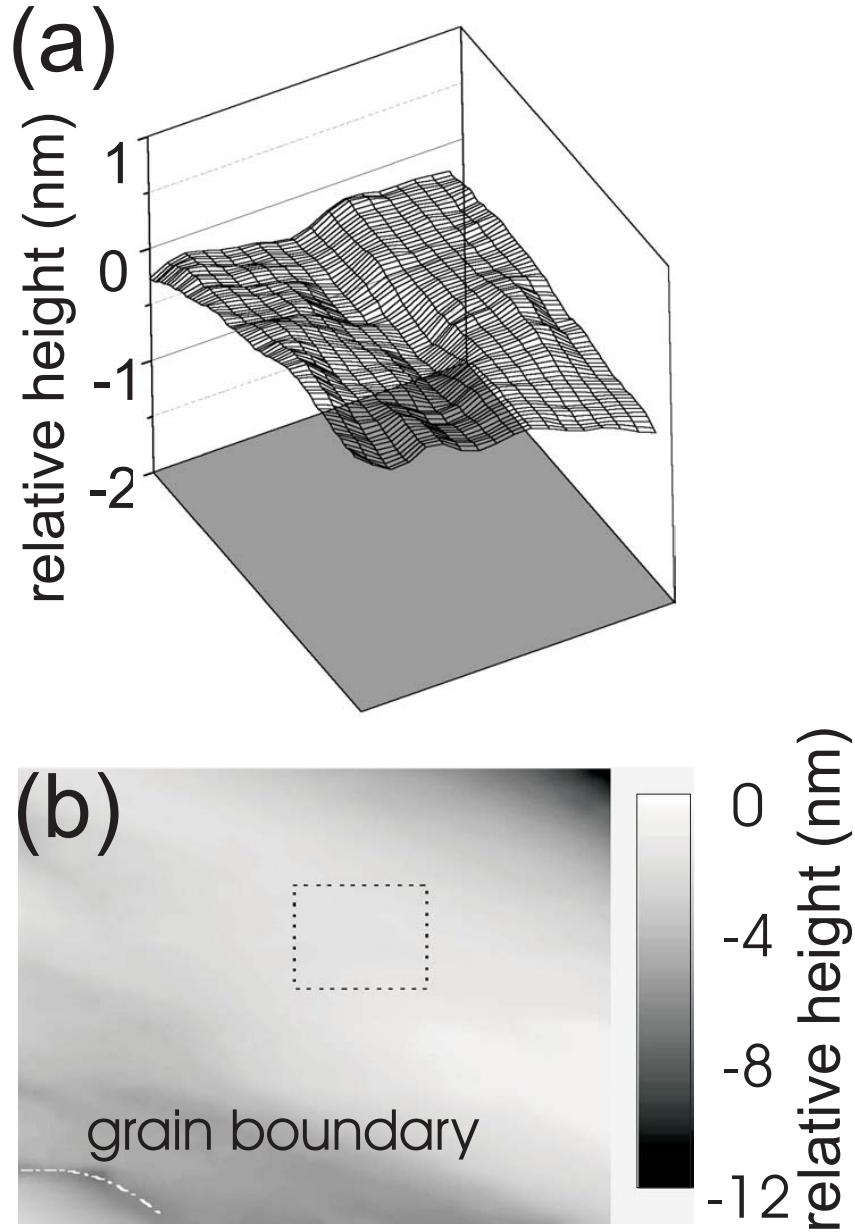


Figure 5.2: (a) A representative surface topography of an area of SLCO with sub-nanometer flatness. The typical area with atomic-scale flatness where most tunneling spectra were taken was greater than $(20 \text{ nm} \times 20 \text{ nm})$, and the work function of the spectra was $0.1 \sim 1 \text{ eV}$. (b) A zoom-out view of the region shown in part (a) (indicated by the dashed box) over an area $(49 \text{ nm} \times 40 \text{ nm})$. Also shown in the lower left corner is a grain boundary.

5.3.1 Pairing symmetry and pairing potential of pure $\text{Sr}_{1-x}\text{La}_x\text{CuO}_2$

A set of representative differential conductance (dI/dV) versus biased voltage (V) spectra for a locally flat area is depicted in Fig. 5.3(a). The waterfall plot displays a line cut of tunneling spectra taken at equally spaced locations with a separation of 1.5 nm. The curves are displaced vertically for clarity except for the bottom curve. We note that the low zero-bias conductance value indicates that the surface disorder is small and the chemical etching procedure is effective.

For the set of data shown in Fig. 5.3(a), both the low-energy spectral gap and the high-energy background are spatially homogeneous up to ~ 100 nm. In general, all spectral characteristics reveal long-range (> 50 nm) spatial homogeneity within each grain. The variations in the spectral gap ($\Delta = 13.0 \pm 2.5$ meV) across hundreds of randomly oriented grains are relatively small, which suggests that the pairing symmetry of SLCO is momentum-independent. Here $(2\Delta/e)$ is defined as the conductance peak-to-peak separation in the spectra. This observation is in sharp contrast to the findings of strongly momentum-dependent spectra in the p-type cuprates with $d_{x^2-y^2}$ pairing symmetry [§4]. The absence of the zero-bias conductance peak (ZBCP), a hallmark for unconventional pairing symmetry, for over 1000 spectra provides additional support for a fully gapped Fermi surface.

By normalizing a typical spectrum in Fig. 5.3(a) relative to the background conductance shown in the left inset of Fig. 5.3(a), we compare the quasiparticle density of states (DOS) of SLCO with the BCS theoretical curve, as illustrated in Fig. 5.3(b). The spectral weight of SLCO for quasiparticle energies at $|E| \geq \Delta$ is smaller than the BCS prediction, whereas excess low-energy DOS appears for $|E| < \Delta$ and the DOS approaches zero at the Fermi level (i.e., $V = 0$). Such behavior cannot be accounted for by the simple inclusion of disorder in the BCS weak-coupling limit, because the latter would have only broadened the width of the conductance peaks and also increased the DOS near $V = 0$ substantially. The spectra also differ fundamentally from those of pure $d_{x^2-y^2}$ -wave cuprates [8] because of the absence of ZBCP and the lack of discernible gap variations in all spectra taken on random grain orientations. Even in a special case of c -axis tunneling, $|d^2I/dV^2|_{V \rightarrow 0^\pm}$ would have been a positive constant in a $d_{x^2-y^2}$ -wave superconductor, as simulated by the thin solid line in

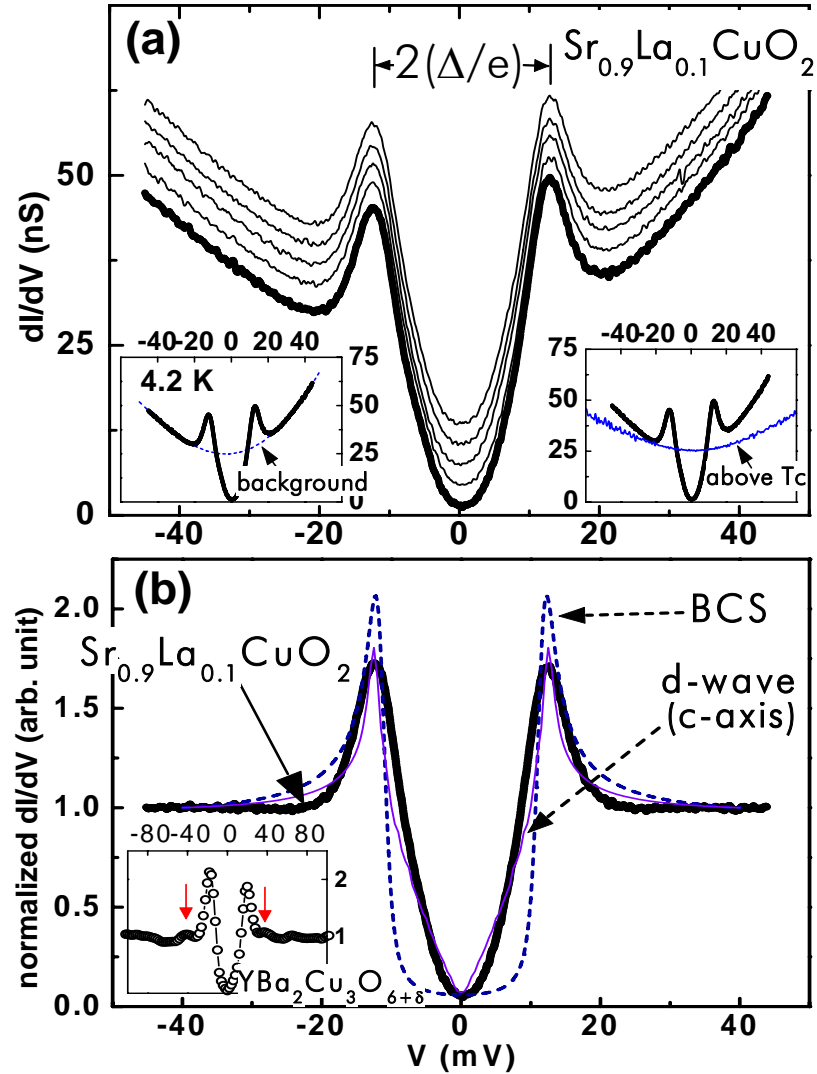


Figure 5.3: (a) Representative (dI/dV) vs. (V) quasiparticle spectra of SLCO taken at 4.2 K. The curves correspond to spectra taken at ~ 1.5 nm equally spaced locations within one grain, and have been displaced vertically for clarity except the lowest curve. Left inset: a typical spectrum taken at 4.2 K (solid line) compared with the corresponding high-voltage background (dashed line). Right inset: comparison of a typical spectrum taken at 4.2 K with one taken slightly above T_c . (b) A spectrum normalized relative to the high-voltage background given in the left inset of (a), together with a BCS theoretical curve for the normalized DOS at $(T/T_c) = 0.1$ and a corresponding c -axis tunneling spectrum for a pure $d_{x^2-y^2}$ -wave superconductor (thin solid line). Left inset: a normalized c -axis tunneling spectrum of an optimally doped $\text{YBa}_2\text{Cu}_3\text{O}_{6+\delta}$ ($T_c = 92.5 \pm 0.5$ K). The red arrows point to the satellite features referred to in the text.

Fig. 5.3(b), which is in contrast to the finding of $|d^2I/dV^2|_{V \rightarrow 0^\pm} = 0$ in SLCO.

In short, the tunneling spectra of SLCO reveal a momentum-independent gap, absence of the Andreev bound state associated with the line nodes and the sign change of unconventional pairing

symmetry, and a smooth change of slope near zero bias as opposed to a discontinuous V-shape in the c -axis tunneling spectra of a d -wave superconductor [Fig. 5.3(b) inset]. These findings are suggestive of isotropic s -wave pairing symmetry. Nevertheless, the excess low-energy excitations signify the breakdown of mean-field BCS theory for the low-energy physics in SLCO, and the unusually large ratio of $(2\Delta/k_B T_c) \approx 7.0$, as compared with the BCS ratio of 3.5, is indicative of strong coupling effects. Interestingly, recent Knight shift data from NMR studies of similar samples have revealed a much smaller normal-state density of states at the Fermi level ($\sim 25\%$ that of YBCO) as compared with those of other cuprates [79], which implies poor screening of the Coulomb repulsion and stronger electronic correlations in SLCO, further corroborating the inapplicability of weak-coupling BCS theory in this system.

5.3.2 Spectral characteristics of pure $\text{Sr}_{1-x}\text{La}_x\text{CuO}_2$

Comparing the tunneling spectra of SLCO with those of the hole-doped YBCO, we find that the commonly observed “satellite features” in the quasiparticle spectra of p-type cuprate superconductors [§4.4.3], as indicated by the arrows in the left inset of Fig. 5.3(b), are invisible in SLCO. Furthermore, when the temperature rises above T_c , the tunneling gap Δ completely vanishes, with no apparent energy scale associated with any depression of the density of states (DOS) at $T > T_c$, as shown in the right inset of Fig. 5.3(a). The normal-state tunneling spectrum remains featureless from just above T_c to ~ 110 K, though the slope of the normal-state high-energy background decreases slightly with increasing temperature due to decreasing conductance with temperature. The absence of any spectroscopic pseudogap in the n-type infinite-layer SLCO is independently verified by the NMR studies on similar samples, showing temperature-independent Knight shift above T_c [79].

The evolution of the tunneling gap with temperature is plotted in Fig. 5.4 for SLCO, PCCO [16], and Bi-2212 [69]. A comparison with the BCS prediction reveals a rapid decrease of spectral gap in SLCO, which is indicative of the deviation from the mean-field description and is consistent with the large $(2\Delta/k_B T_c) \approx 7.0$ ratio found in this system. We note that the temperature dependence of the tunneling gap in NCCO [41] (not shown) and PCCO [16] is well captured by the BCS theory

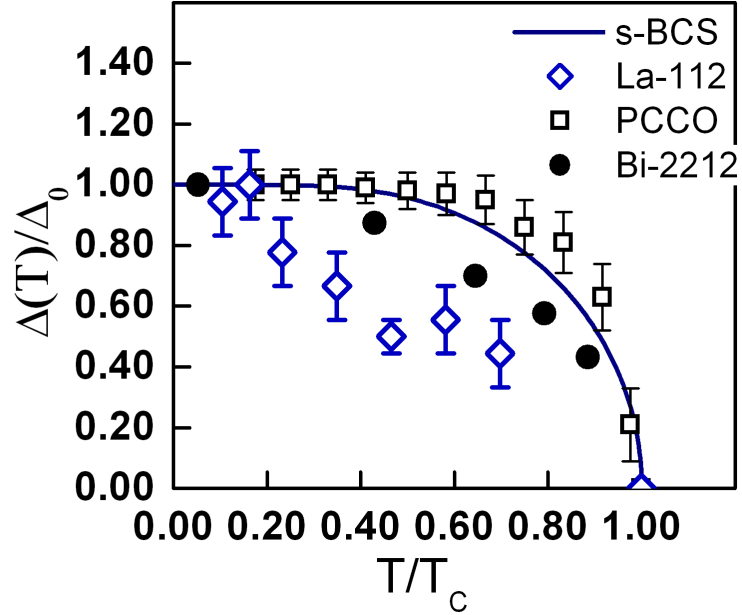


Figure 5.4: Comparison of the temperature dependence of the normalized spectral gap for PCCO [16], Bi-2212 [69] and SLCO. $\Delta(T)$ is the spectral gap measured at temperature T , and Δ_0 represents the zero temperature tunneling gap.

with an s -wave pairing. A detail analysis of the NCCO tunneling spectra using the BTK formalism yields a nearly perfect fit with $(2\Delta/k_B T_c) \approx 3.3$ [41] comparable to the BCS value.

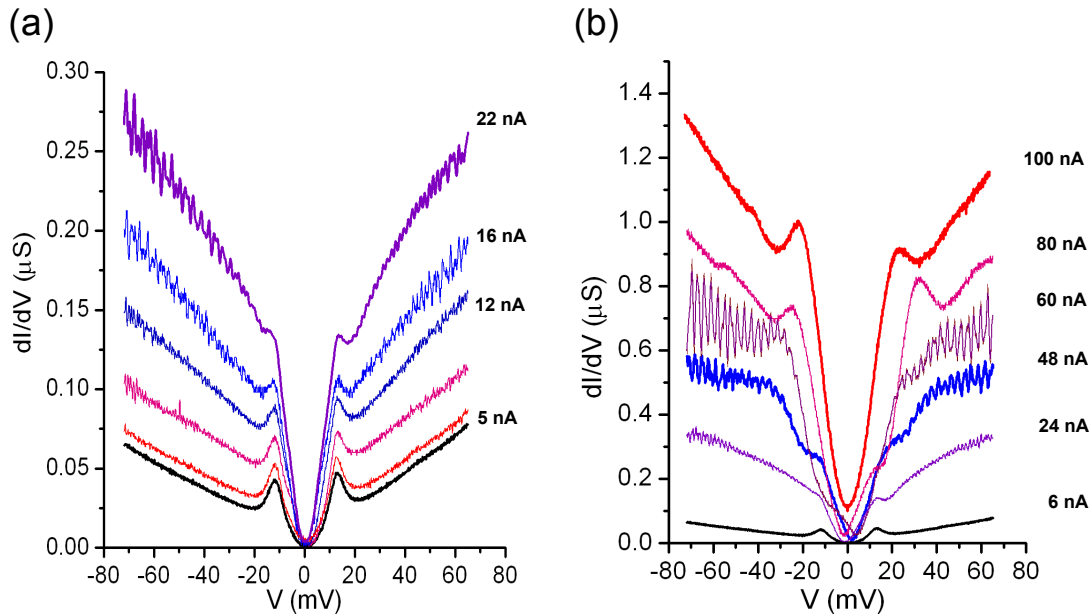


Figure 5.5: The evolution of tunneling spectra with increasing injection current.

In Figure 5.5, an interesting phenomenon associated with the current dependence of the tunneling

spectra is depicted. Each spectrum is labeled by its corresponding set-point tunneling current at the fixed-bias voltage, 100 mV, and taken with the feedback loop disabled so that the tunneling matrix is kept at a constant value within each acquisition. The spectra acquired at lower injection current values show that the height of the spectral peaks slowly reduced with increasing current, whereas the energy gap value remains the same. The sharp spectral peaks indicative of quasiparticle coherence persist up to $I \leq \sim 22$ nA and are fully suppressed as the injection current passes ~ 24 nA. A broad high-energy “pseudogap”-like feature emerges and gradually dominates over the remnant low-energy feature. After the low-energy gap completely disappears, the “pseudogap” sharpens up whereas the gap value slightly decreases to ~ 23 meV at $I = 100$ nA.

We note that the spectral response to large injection current is fully reversible, with the high-energy “pseudogap” vanishing and the low-energy gap recovering with decreasing tunneling current, as exemplified by the bottom curve in Fig. 5.5(b). Therefore, it is unlikely that the injection current induces structural or chemical changes that give rise to the spectral changes. Further, we can rule out local heating as the cause of the anomalous current-induced “pseudogap” because, as shown in Fig. 5.4, the low-energy superconducting gap decreases rapidly with increasing temperatures, as opposed to the large “pseudogap” revealed by high current injection.

The spectral characteristics of the tunneling spectra under large current injection are reminiscent of those observed in the pseudogap phase of the underdoped p-type cuprates. Thus, we speculate that, similar to the high-energy satellite features in the superconducting spectra of p-type cuprates, the current-induced “pseudogap” is indicative of the underlying coexisting state, where the superconductivity is gradually suppressed while the strength of the competing order promoted with increasing current [§5.4.3].

5.3.3 Tunneling spectra of Zn- and Ni-doped $\text{Sr}_{1-x}\text{La}_x\text{CuO}_2$

The tunneling spectra taken on the 1% Zn-doped SLCO reveal long-range spatially homogeneous spectral characteristics and a similar gap value ($\Delta = 13.0 \pm 2.5$ meV) for randomly sampled areas in different grains, as exemplified in Fig. 5.6. Given that the average separation among Zn

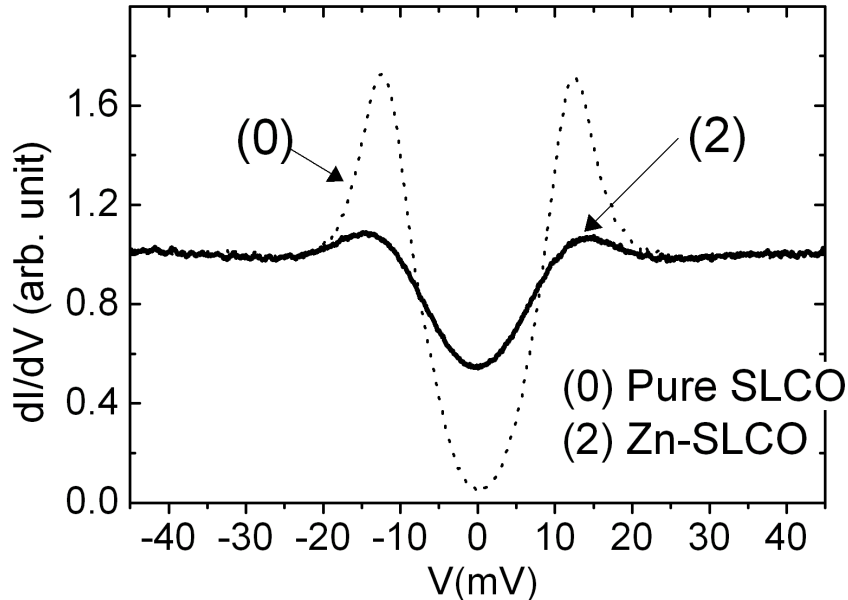


Figure 5.6: Comparison of quasiparticle tunneling spectra of 1% Zn-SLCO and pure SLCO, showing significant residual conductance in the subgap region and broadened spectral peaks indicating reduced quasiparticle lifetime due to disorder for the Zn-SLCO.

impurities is $\sim (1.8 \times 1.8 \times 1.6) \text{ nm}^3$, our exhaustive spectral studies should have covered a significant number of Zn impurities. However, no significant local variations are found in the spectra of the 1% Zn-SLCO, which differs fundamentally from our observation of atomic-scale spectral variations in a $\text{YBa}_2(\text{Cu}_{0.9934}\text{Zn}_{0.0026}\text{Mg}_{0.004})_3\text{O}_{6.9}$ single crystal near non-magnetic Zn or Mg impurities [Fig. 4.3.2]. Nevertheless, the conductance peaks in 1% Zn-SLCO are significantly broadened relative to pure SLCO, with a substantial increase in the low-energy DOS for $|E| < \Delta$, as illustrated in Fig. 5.6. These features suggest that Zn impurities result in reduced quasiparticle lifetime while retaining T_c , similar to the response of conventional s -wave superconductors to non-magnetic impurities [211, 244].

In contrast, two types of spectra are observed in 1% Ni-SLCO, As illustrated in the main panel of Fig. 5.7(a), the majority spectra ($> 90\%$) exhibit suppressed coherence peaks, large zero bias residual conductance, strong electron-hole spectral asymmetry, and gradual spatial evolution over a long range. In contrast, the minority spectra ($< 10\%$) exhibit sharp spectral peaks, small zero-bias conductance, and varying electron-hole spectral asymmetry over a short range ($< 1 \text{ nm}$), as

exemplified in the inset of Fig. 5.7(a) for two representative minority spectra. The significant spectral asymmetry in the majority spectra implies different phase shifts in the electron-like and hole-like quasiparticle states as the result of broken time-reversal symmetry [244, 212], which may be responsible for the global suppression of the superconducting phase coherence and thus a reduction in T_c .

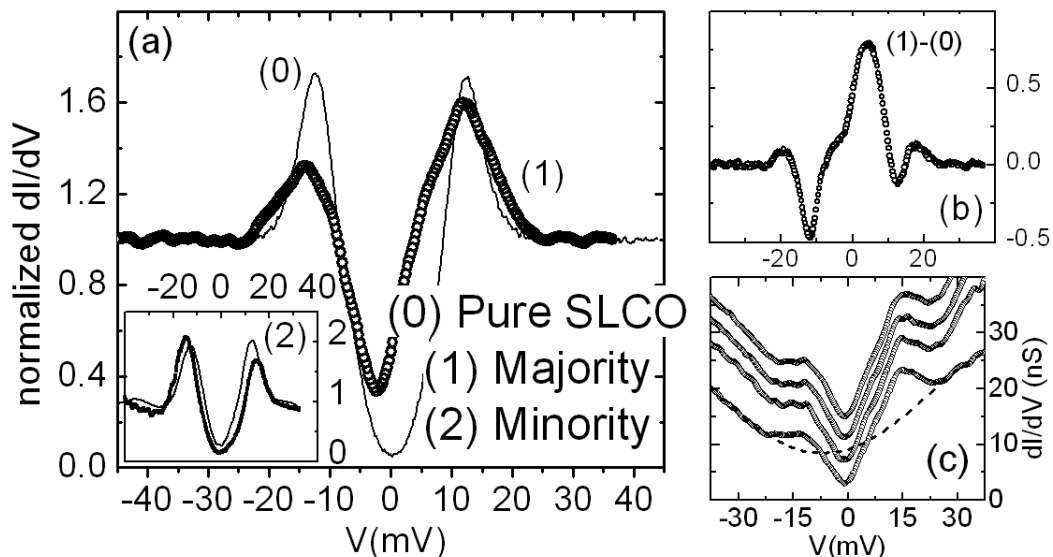


Figure 5.7: (a) Main panel: Comparison of a normalized majority spectrum of 1% Ni-SLCO and that of pure SLCO at 4.2 K. The normalization was made relative to the background conductance shown by the dashed line in part (c). Inset: Two minority spectra with different electron-hole asymmetry. (b) Spectral differences of the majority and minority spectra relative to that of the pure SLCO. (c) A series of spectra taken on the same grain of 1% Ni-SLCO at ~ 3 nm apart. The conductance of all curves except the lowest one has been displaced up for clarity.

Assuming homogeneous Ni impurity distributions, the average Ni-Ni separation would be $d_{Ni} \sim 1.8$ nm in the ab -plane and ~ 1.6 nm along the c -axis in each grain. The impurity wavefunction with poor screening from the carriers would have extended over a coherence volume ($\xi_{ab}^2 \xi_c$) [244, 212]. Given the coherence lengths $\xi_{ab} \sim 4.8$ nm and $\xi_c \sim 0.53$ nm [241], $\sim 30\%$ volume probability in each grain could be considered as under significantly weaker impurity influence. In the limit of completely random grain orientation in 1% Ni-SLCO, the STM studies of the grain surfaces would have 10–20% probability for finding surface regions with weak impurity influence and spatial extension over a short range (~ 0.5 nm) along the c -axis. This simple estimate is in reasonable agreement with our observation of $\sim 10\%$ minority spectra with short-range (< 1 nm) spatial homogeneity. However,

due to the lack of direct information for the Ni distribution on the sample surface, the true origin for two types of spectra in 1% Ni-SLCO remains uncertain.

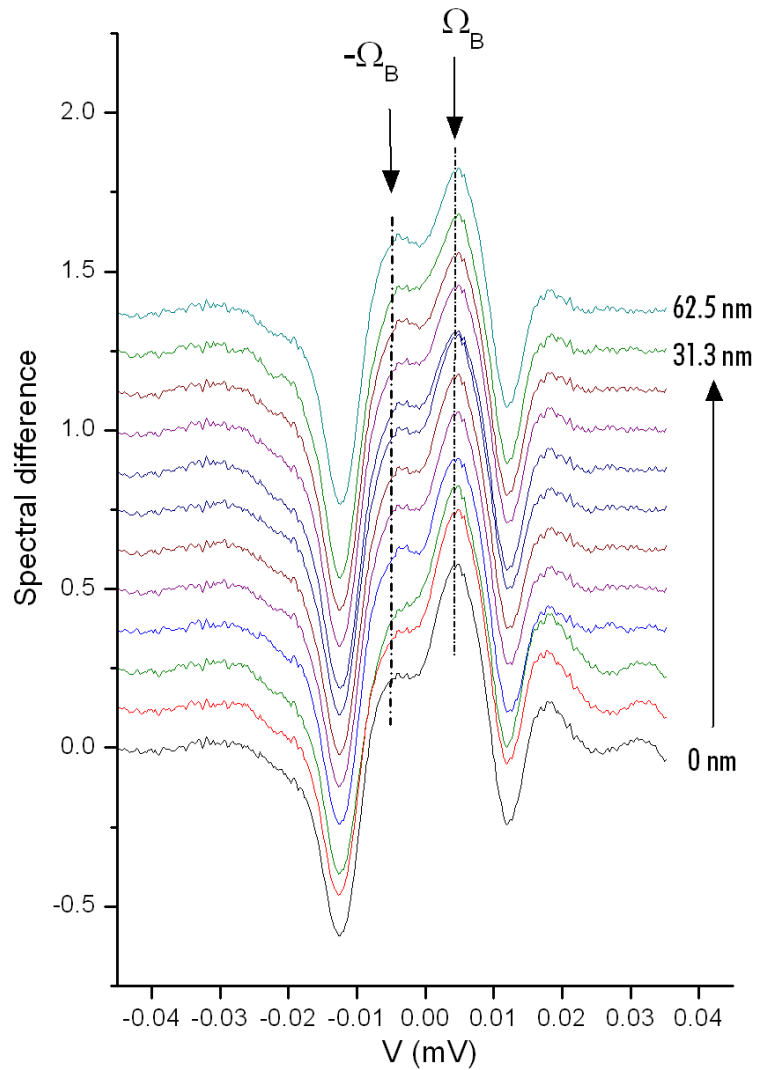


Figure 5.8: The spatial evolution of the spectral difference in the vicinity of the Ni impurity, showing long-range impurity bound states at energy $\pm\Omega_B$ similar to the Shiba states of the magnetic impurity bands in a conventional superconductor.

Considering the spectral difference between the majority spectrum of 1% Ni-SLCO and that of pure SLCO [Fig. 5.7(b)], we find that the spectral characteristics resemble the findings in Ref. [244] and are representative of magnetic impurity-induced state. Since the average Ni-Ni separation (~ 1.8 nm) is smaller than the in-plane coherence length (~ 4.8 nm), the Ni impurities can be considered as forming a magnetic impurity band. According Shiba's theory [245], the bound state energy

associated with the Ni-impurity band in an s -wave superconductor locates at $\pm\Omega_B$ as depicted in Fig. 5.8, where a set of spectra illustrating the slow variations in spectral difference around the Ni impurity is given. The weak screening owing to the low carrier density and the strong overlap of impurity wavefunctions explain the slow-varying spectra shown in Fig 5.7(c) and Fig. 5.8.

5.4 Discussion

5.4.1 Pairing symmetry

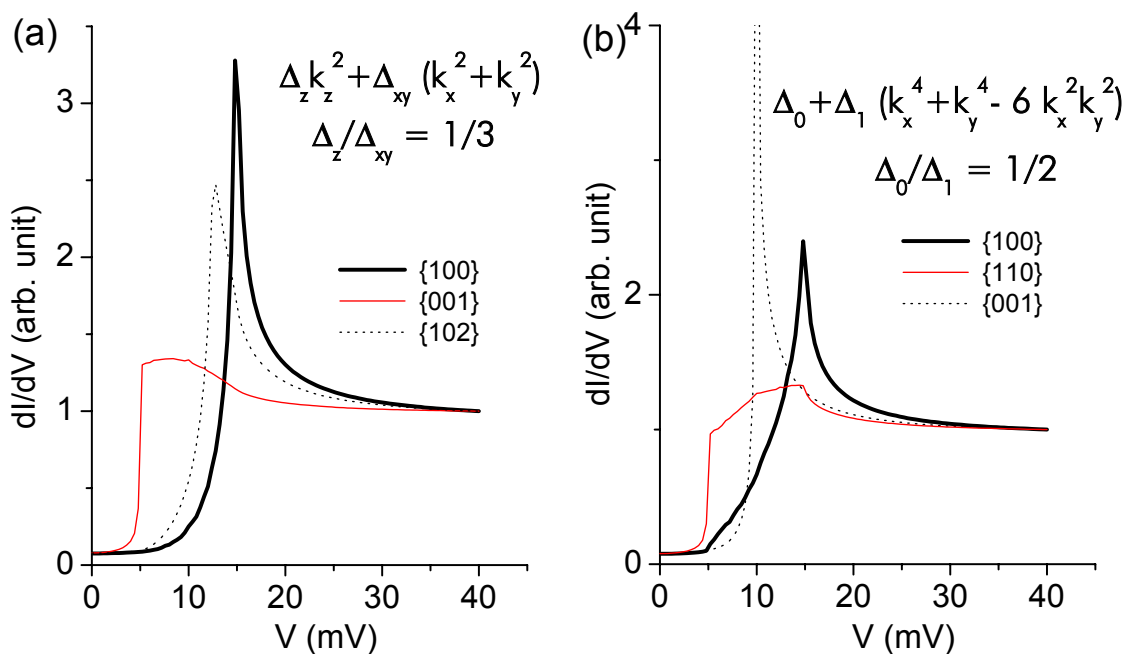


Figure 5.9: Simulated tunneling spectra along different crystalline axes for (a) an anisotropic s -wave pairing with uniaxial symmetry $\Delta_{\vec{k}} = \Delta_{xy}(k_x^2 + k_y^2) + \Delta_z k_z^2$, and (b) an anisotropic s -wave pairing with four-fold in-plane modulation $\Delta_{\vec{k}} = \Delta_0 + \Delta_1(k_x^4 + k_y^4 - 6k_x^2 k_y^2)$.

The lack of spectral variations with crystalline orientations, the absence of ZBCP, and the distinctly different bulk and local spectral response to non-magnetic and magnetic impurity substitution suggest that SLCO is a fully gapped s -wave superconductor. To explore the possibility of any anisotropy in the pairing symmetry, we use the generalized BTK formalism to derive the tunneling spectra for the anisotropic order parameters permitted by the crystalline symmetry. In the case of the infinite-layer SLCO, the point group of the lattice is D_{4h} . We consider the lowest energy con-

figurations of the order parameter with orbital angular momenta $l = 0, 2, 4$. For $l = 0$, the pairing symmetry is isotropic s . For $l = 2$ and $l = 4$, the relevant anisotropic pairing potentials are the uniaxial symmetric anisotropic s -pairing, $\Delta_{\vec{k}} = \Delta_{xy}(k_x^2 + k_y^2) + \Delta_z k_z^2$, and the in-plane four-fold symmetric anisotropic s -pairing, $\Delta_{\vec{k}} = \Delta_0 + \Delta_1(k_x^4 + k_y^4 - 6k_x^2 k_y^2)$. The calculated spectra of anisotropic s -wave superconductors with quasiparticles tunneling along different crystalline axes are illustrated in Fig. 5.9. For tunneling spectra taken on randomly oriented crystallites of an anisotropic s -wave superconductor, the variations in the tunneling gap values can be resolved if the anisotropy in the pairing potential is appreciable. By comparing the numerical result with the STS data and taking into account the experimental resolution, we estimate that the upper bound for the anisotropy of the pairing potential is less than 8%, so that the pairing potential of SLCO is essentially isotropic.

5.4.2 Impurity substitution and pairing symmetry

An important consequence of either $d_{x^2-y^2}$ or $(d_{x^2-y^2} + s)$ -wave pairing is that the resulting nodal quasiparticles can interact strongly with the quantum impurities in the CuO_2 planes [214, 213, 246], such that a small concentration of impurities can lead to strong suppression of superconductivity. The scattering of quasiparticles by the non-magnetic impurities dramatically modifies the local spectral response, yielding a low-energy resonance feature while suppressing the superconducting coherence peaks [8, 220] as observed in the tunneling spectra of (Zn,Mg)-YBCO [§4.3.2]. Furthermore, the induced magnetic moments that are confined to the vicinity of the non-magnetic impurities [215, 247, 216, 217, 218] can couple with the Bogoliubov quasiparticles and give rise to Kondo physics [222, 219]. Such strong response to non-magnetic impurities is in sharp contrast to that of conventional s -wave superconductivity [211, 244].

In comparison, the T_c of the infinite-layer SLCO has little dependence on the non-magnetic Zn substitutions up to 3%, but it is drastically suppressed with only 1% of magnetic Ni substitutions [243]. Figure 5.10 illustrates the suppression of T_c upon impurity substitution observed by the bulk susceptibility measurements. While 1% of Zn substitutions hardly changes the transition temperature, 1% of Ni substitutions decreases T_c from 43 K to ≤ 32 K. With 2% of Ni substitutions,

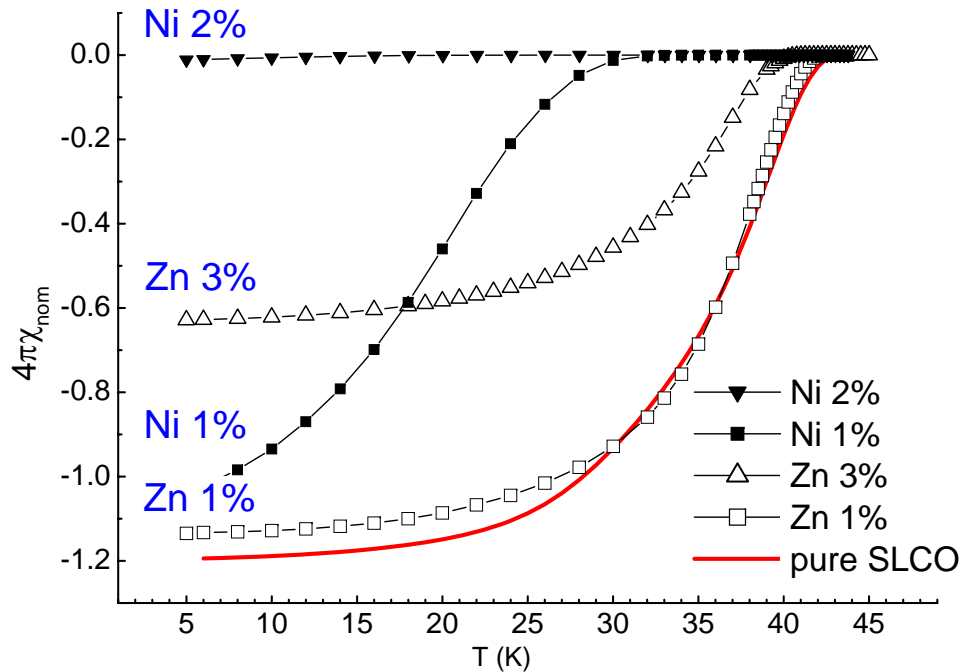


Figure 5.10: (Adapted from Fig. 1(b) of Ref. [240].) Magnetic susceptibility data of pure and impurity doped SLCO. The superconducting transition temperature has little variation upon Zn doping up to 3%, while superconductivity is completely suppressed with 2% of Ni doping.

superconductivity is completely suppressed. Thus, the global response of SLCO to impurities is different from that in the p-type cuprates and is similar to that in an *s*-wave superconductor [211].

Microscopically, the effect of non-magnetic Zn impurities on the tunneling spectra [Fig. 5.6] can be accounted for with the increase of the quasiparticle lifetime broadening which smears out the superconducting peaks without changing the nature of the eigenstates, a behavior completely different from that in a *d*-wave superconductor where resonance bound states associated with impurity scattering are generally observed.

In comparison, the majority spectra [Fig. 5.7] found in the 1% Ni-SLCO show strong electron-hole asymmetry with spectral contributions from the magnetic impurities reminiscent of those in an *s*-wave superconductor [244]. However, the slow spatial variations in Ni-SLCO due to weak screening effects and strong overlapping of Ni wavefunctions are markedly different from the rapidly diminishing impurity bound states observed near the isolated Mn or Gd atom on the surface of the conventional superconductor Nb [244] and also from the strong atomic-scale spectral variations near Ni impurities in the p-type cuprate $\text{Bi}_2\text{Sr}_2\text{Ca}(\text{Cu}_{1-x}\text{Ni}_x)_2\text{O}_{8+x}$ [248]. The contrast in the spatial extension of the

Ni-impurity effects may be attributed to the variation in the impurity coupling strength and range, and also to the degree of impurity screening by carriers. Overall, both bulk and microscopic studies of Zn and Ni substituted SLCO corroborate our findings on pure SLCO that the infinite-layer n-type cuprate superconductors exhibit *s*-wave pairing symmetry.

5.4.3 Satellite features, pseudogap phenomena, and competing orders

In the previous chapter [§4.4.3], we have mentioned that the “dip-hump” features in the tunneling spectra of hole-doped cuprates are generally attributed to quasiparticle interaction with background bosonic excitations. Within the quasiparticle damping scenario, there are two possible bosonic modes in the cuprate superconductors that quasiparticles can couple to. One is the magnetic resonance mode, and the other is the phonon mode. A recent study of the angular-resolved photoemission spectroscopy (ARPES) on Bi-2212, Pb-doped Bi-2212, Pb-doped $Bi_2Sr_2CuO_6$, and LSCO reveals an abrupt change of the electron group velocity in the 50 ~ 80 meV energy range [206]. The similar energy scales exhibited in these four different systems prompt some physicists to speculate that the longitudinal optical oxygen phonon modes in the CuO_2 planes are responsible for the change of slope in the quasiparticle dispersion [206] and the satellite features in tunneling spectra. However, as shown in §4.4.3, it is unlikely that the satellite features are associated with the phonon modes, since the strong suppression of the “dip” energy observed in (Zn,Mg)-YBCO [8] and the significant reduction of the electron self-energy in Bi-2212 [210] upon impurity substitution with similar atomic masses cannot be reconciled with the phonon mediation scenario. On the other hand, the energy of the resonance mode extracted from the Bi-2212 tunneling spectra are consistent with the resonant energy measured by magnetic neutron scattering measurements [149], thereby providing convincing evidence for the magnetic damping scenario in Bi-2212.

Besides the high-energy “dip-hump” features, additional *lower-energy* satellite features are revealed in the tunneling spectra of underdoped Bi-2212 [183, 220, 68] at an energy scale comparable to the pseudogap observed above T_c . These low-energy features sometimes dominate over the superconducting sharp peaks and form the pseudogap-like spectra [68] [Fig. 6.4(d)]. The coexistence

of these pseudogap-like features with the pure superconducting spectra suggests that they are the manifestation of the competing orders in the underdoped Bi-2212. The tunneling spectra on YBCO exhibit similar lower-energy spectral features at energies slightly above the superconducting gap. If we attribute these lower-energy satellite features to the magnetic resonance mode in YBCO, the resonance frequency from the tunneling experiment would be appreciably smaller than that obtained from the neutron scattering results [83] (*cf.* inset of Fig. 5.10(a)). For this reason, we propose to interpret the satellite features in YBCO as a manifestation of coexisting competing orders.

For a competing order strength comparable to or larger than the superconducting pairing potential, the spectral gap of the coexisting state would take place at an energy slightly higher than the superconducting gap, which corresponds to the satellite features in the superconducting state of YBCO and Bi-2212. Furthermore, as the stiffness of the competing order increases while that of superconductivity decreases with underdoping, the spectral gap associated with the competing order would sustain beyond the superconducting transition temperature, giving rise to the pseudogap observed in the normal of the underdoped p-type cuprates.

On the other hand, if the strength of the competing state is small compared to the superconducting pairing potential, the spectral gap associated with the coexisting competing order would be buried in the pronounced superconducting peaks and rendered invisible, which accounts for the absence of satellite features in the electron-doped infinite-layer SLCO and one-layer compounds. Furthermore, as the temperature increases, the coexisting order would vanish before superconductivity disappears, which explains why no discernible pseudogap is observed above T_c .

The absence of the zero-field pseudogap in SLCO is consistent with similar findings in the one-layer electron-doped NCCO and PCCO [16, 18]. It is shown that, in the one-layer systems, the application of a magnetic field that destroys superconductivity reveals a suppression of DOS near the Fermi level in the field-driven normal state [18], which signifies the existence of a competing order. By taking into account the spectral smearing, it is found that the strength of the field-induced pseudogap is smaller than the zero-temperature superconducting gap, which accounts for the observation that the onset temperature of the “pseudogap” opening in the field-driven normal

state is smaller than the superconducting transition temperature in zero field.

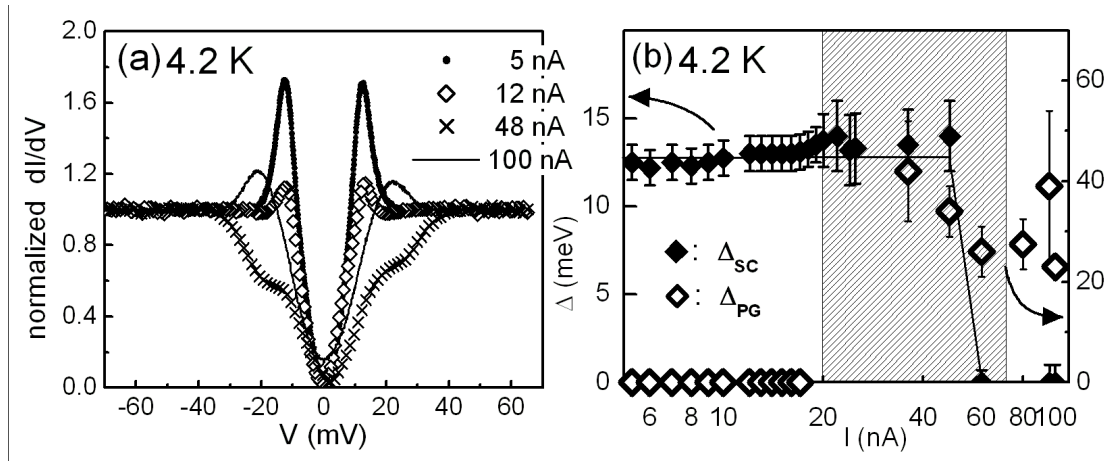


Figure 5.11: (a) Representative normalized quasiparticle tunneling spectra of SLCO with increasing tunneling current I . (b) Evolution of the low-energy superconducting gap Δ_{SC} and the high-energy current-induced pseudogap Δ_{PG} of SLCO with I . The shaded region is where quantum fluctuations are strong and the two orders coexist.

The current-induced “pseudogap” in the tunneling spectra of SLCO can be understood within the same picture. Figure 5.11(a) shows a set of representative normalized spectra taken from Fig. 5.5. In the low-current limit, superconductivity dominates over the competing order so that there are no discernible satellite features, the appearance of which would have been indicative of a competing order energy scale exceeding that of superconductivity. As the current increases, the Bogoliubov quasiparticles gradually lose coherence (as manifested by the diminished coherence peaks) probably due to increasing local fields induced by the large tunneling currents, and the competing order gains strength. When the magnitude of the competing order becomes significant, the high-energy satellite features emerge at the energy $\Delta_{PG} \sim \sqrt{\Delta_{SC}^2 + V_{CO}^2}$ and coexist with the low-energy remnant gap Δ_{SC} [Fig. 5.5(b)]. Eventually, the injection current renders the superconducting order parameter sufficiently small, and the high-energy “pseudogap” dominates over the negligible remnant superconducting gap. A rigorous theoretical foundation for the notion described here will be provided in Chapter 6.

Thus, by tuning the relative strength of the competing order to superconductivity, the presence of the zero-field pseudogap in p-type cuprates, and the field- and current-induced pseudogap in n-type

cuprates can be explained in a coherent way.

5.4.4 Low-energy excitations, quantum fluctuations, and quantum criticality

We have noted in §5.3.1 that despite the observation of the momentum-independent quasiparticle tunneling spectra supportive of s -wave pairing symmetry, the spectral characteristics of SLCO deviate significantly from the conventional s -wave BCS prediction [Fig. 5.3(b)]. The excess low-energy excitations manifested in the low-temperature quasiparticle spectra are indicative of substantial quantum fluctuations resulting from the presence of a competing order close in energy to superconductivity.

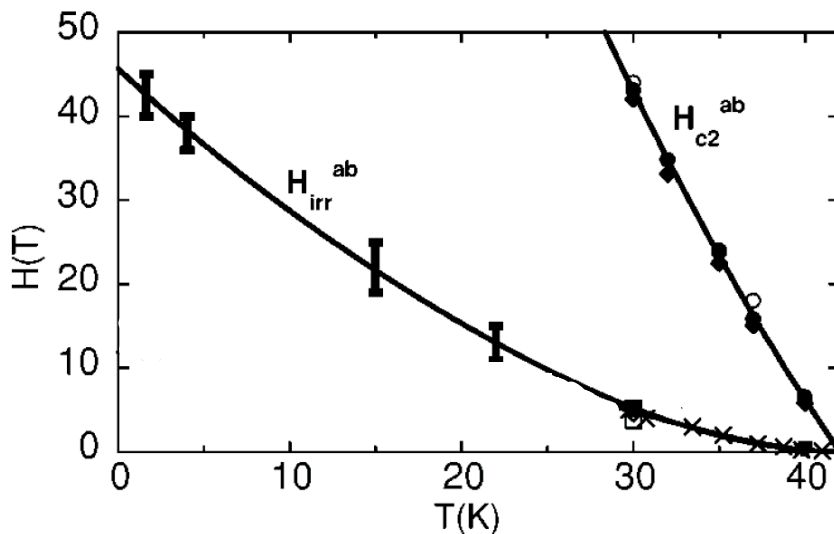


Figure 5.12: (Adapted from Fig. 3 of Ref. [107].) The vortex phase diagram of electron-doped infinite-layer SLCO for $H \parallel ab$ showing significant reduction of the in-plane irreversibility field (H_{irr}^{ab}) relative to the in-plane higher critical field (H_{c2}^{ab}).

High-field vortex dynamics measurements on SLCO provide additional evidence for strong quantum fluctuations [107, 201, 202]. These experiments are conducted with the magnetic field parallel to the CuO_2 planes, so that the fluctuations due to disorder pinning are minimized by the strong confinement of vortices along the periodic CuO_2 planes. In the absence of quantum fluctuations, the in-plane irreversibility field (H_{irr}^{ab}) is expected to approach the in-plane upper critical field (H_{c2}^{ab}) as $T \rightarrow 0$, where thermal depinning mechanism is quenched. Therefore, our experimental finding of a

large reduction of $H_{irr}^{ab}(T \rightarrow 0)$ relative to $H_{c2}^{ab}(T \rightarrow 0)$ in SLCO [Fig. 5.12] must be attributed to field-induced quantum fluctuations that suppress the phase stiffness of superconductivity. Specifically, large magnetic fields induce strong transverse phase fluctuations that suppress superconductivity phase coherence and enhance the competing order even at $T = 0$. Thus, the strong quantum phase fluctuations prevent the superconductor from supporting a well-defined supercurrent in high fields, leading to $H_{irr}^{ab}(T = 0) < H_{c2}^{ab}(T = 0)$. On the other hand, although transverse phase fluctuations are negligible in the zero-field limit at $T = 0$, the coupling of quasiparticles with longitudinal quantum phase fluctuations can account for the excess low-energy spectral weight manifested in the tunneling spectrum [§6].

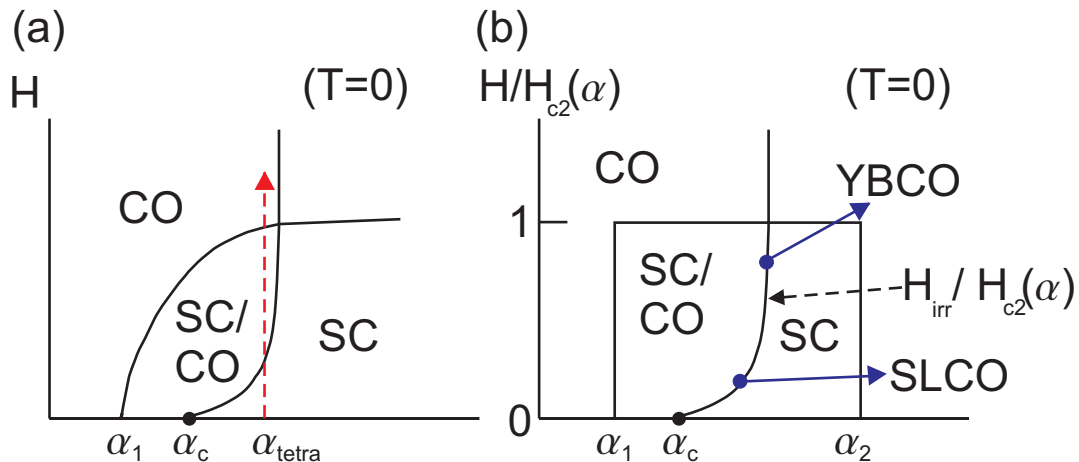


Figure 5.13: (a) Schematic H vs. α phase diagram at $T = 0$ showing the field-induced quantum phase transition from a superconducting phase with a dynamic competing order to a coexisting phase with superconductivity and a static competing order. α : relevant material specific parameter, such as doping level, disorder, electronic anisotropy and on-site Coulomb repulsion; α_i ($i = 1, 2, c$): quantum critical point; α_{tetra} : tetra-critical point; SC/CO: superconducting phase with coexisting static competing order; SC: superconducting phase (with coexisting dynamic competing order when $\alpha < \alpha_{tetra}$). (b) Reduced field $H/H_{c2}(\alpha)$ vs. α phase diagram at $T = 0$ showing the relative proximity to the quantum critical point α_c for SLCO and YBCO.

We can further use the degree of quantum fluctuations extracted from the high-field thermodynamic measurements to characterize the proximity to quantum criticality for individual cuprate compounds. Theoretical investigations [249, 250, 251] indicate that in the presence of a competing order energetically comparable to superconductivity, the application of a magnetic field would induce a phase transition from the coexisting phase with the dynamic competing order to one with

static long-range order [Fig.5.13(a)]. In the vicinity of the critical line where the fluctuations of the competing order are significant, the superconducting order parameter that couples with the competing order [252] would also fluctuate substantially. Therefore, by examining the suppression of H_{irr}^{ab} with respect to H_{c2}^{ab} in the zero-temperature limit for various cuprate compounds, we can map out their relative proximity to quantum criticality. Comparing the high-field vortex phase diagram of SLCO [107] to that of YBCO [253, 254], we find that SLCO is much closer to the quantum critical point than YBCO [Fig.5.13(b)], and therefore the low-energy excitation spectra of SLCO deviate considerably from the mean-field BCS theory, while that in YBCO is well described by the mean-field generalized BTK theory.

5.5 Summary

In conclusion, we present the quasiparticle tunneling spectra of the electron-doped infinite-layer cuprate SLCO that demonstrate a momentum-independent pairing potential $\Delta = 13.0 \pm 2.5$ meV with an anisotropy $< 8\%$. The global and local spectral response to impurity substitution is consistent with s -wave pairing symmetry. The absence of satellite features, the absence of zero-field pseudogap, and the emergence of the current-induced pseudogap suggest that, in SLCO, superconductivity coexists with a small fluctuating competing order revealed only upon the suppression of superconductivity by external perturbations. The proximity of the ground state to the quantum critical point gives rise to significant quantum fluctuations, as manifested in the high-field vortex dynamics measurement. The coupling of quasiparticles to the quantum phase fluctuations of the superconducting order parameter results in excess low-energy excitations observed in the tunneling spectra. We shall present further supporting evidence from the theoretical modeling of quasiparticle tunneling spectra in the presence of strong quantum fluctuations and competing orders in the following chapter.